Suppressed Reflection of Electric Fields Induced in a Stressed X-Point Collapse*)

Takayuki HARUKI, Naru TSUJINE[1)], Shota YONEZAWA[1)] and Masahiro SATO

Graduate School of Science and Engineering, University of Toyama, Toyama 930-8555, Japan

[1)]*Graduate School of Science and Engineering for Education, University of Toyama, Toyama 930-8555, Japan*

(Received 10 January 2019 / Accepted 9 March 2019)

Magnetic reconnection is a basic physical process in which the magnetic field energy is converted into plasma heating and plasma kinetic energy through non-thermal particle acceleration. To investigate collisionless magnetic reconnection, particle-in-cell (PIC) simulations of a stressed (magnetic) X-point collapse have been performed, and the simulation results are highly similar to those obtained for the well-known Harris-type current sheet model. However, through careful study, we found that the stressed X-point configuration initially induces electric fields, which propagate outward, are reflected from the simulation boundaries, and then influence the reconnection physics. In this study, we performed precise PIC simulations of a stressed X-point collapse by introducing an absorption region. The results show that the electric fields propagating outward are damped in the absorption region and their reflection from the boundaries is largely suppressed. The influence of the reflected electric fields on the X-point is therefore removed from the system. Hence, the introduction of an absorption region is highly effective for investigating the physics of a stressed X-point collapse.

Keywords: magnetic reconnection, X-point, particle-in-cell simulation, absorption region

DOI: 10.1585/pfr.14.3401076

1. Introduction

Magnetic reconnection is a basic physical process in which the magnetic field energy is converted into plasma heating and plasma kinetic energy through non-thermal particle acceleration [1, 2]. This physical phenomenon is observed in a variety of fields, ranging from astrophysics to fusion plasma. In particular, a reconnection electric field that appears in a kinetic regime has the potential to directly accelerate plasma particles in addition to a traditional reconnection outflow. To investigate magnetic reconnection, a number of numerical simulations have been performed using the well-known Harris-type current sheet model, where anti-parallel magnetic fields are initially established, between which a current sheet arises.

The Geospace Environment Modeling (GEM) challenge demonstrated important results for the Harris-type current sheet [3]. In this project, a variety of numerical codes were used to model collisionless magnetic reconnection. It was reported that the reconnection rate does not depend on the code used as long as the Hall effect is included in the system. Among these efforts, Pritchett performed particle-in-cell (PIC) simulations [4]. Different diffusion regions for electrons and ions were observed, and an out-of-plane quadrupole magnetic field was produced by the Hall effect. The reconnection electric field produced in the vicinity of an X-point is primarily supported by the off-diagonal components of the electron pressure term in the generalized Ohm's law. These results are still useful for understanding the physics of reconnection.

In addition, PIC simulations for a stressed X-point (a so-called null point) collapse were performed to elucidate the reconnection physics for an X-point [5, 6]. In this model, the initial magnetic stress, determined by the initial X-point magnetic field configuration, causes the system to collapse. The magnetic stress is controlled by the stress parameter α in the initial magnetic fields equations. By changing the stress parameter α ($\geq$ 1), we can control the degree of the X-point collapse. These simulation results are highly similar to those reported for the Harris-type current sheet model. The reconnection electric field is supported by the off-diagonal terms of the electron pressure tensor, similar to the GEM reconnection challenge results. Other studies also considered the effect of a guide field (an initial out-of-plane magnetic field) in a stressed X-point collapse [7, 8]. An octupolar magnetic field structure was also recently proposed, and its mechanism was investigated [9, 10].

Recently, the trajectories of individual particles have been analyzed near reconnection regions for a Harris-type current sheet [11]. In PIC simulations, electrons and ions are treated as particles, where plasma distribution functions in phase space and individual particles can be tracked in detail. It has been proposed that electron trajectories are classified by whether they cross the reconnection region

author's e-mail: haruki@sus.u-toyama.ac.jp

*) This article is based on the presentation at the 27th International Toki Conference (ITC27) & the 13th Asia Pacific Plasma Theory Conference (APPTC2018).

or not. This method of classification for studying the dynamics of energetic particles in detail is applicable for the stressed X-point model.

In our experiments, we found that the stressed X-point configuration initially induces electric fields, which propagate outward and are then reflected from the simulation boundaries. We believe that these initially induced electric fields result from a non-equilibrium initial state in the stressed system. However, the reflection of electric fields from the boundaries influences the reconnection physics in the vicinity of the X-point. In particular, particles (primarily electrons) are likely to be abnormally accelerated by the reflected electric fields, making it difficult to analyze the behavior of energetic plasma particles.

In this study, we aim to perform precise PIC simulations of a stressed X-point collapse by introducing an absorption region [12]. We superimposed the absorption region on the simulation model used in the previous study to suppress the reflection of the electric fields propagating outward. For a simple implementation of an absorption region, we used the masking method, which can dampen the amplitude of waves as a function of distance from the X-point.

In this paper, our simulation model is described in Section 2. In Section 3, our simulation results are shown and compared with the results of a previous study. In Section 4, we draw conclusions from our simulation study.

2. Simulation Model

The numerical code used here is a two-dimensional (2-D), relativistic, fully electromagnetic PIC code modified from the *TRISTAN* code [13]. We previously translated the original FORTRAN code into C/C++ to improve the code's versatility via the use of a modern object-oriented design.

2.1 Governing equations

In PIC codes, the electrons and ions are modeled not as fluids but rather directly as particles. The charged particles are free to move throughout the numerical domain, and the electromagnetic fields are defined at grid or half-grid points.

The governing equations are the equations of motion for each particle and Maxwell's equations:

$$\frac{\mathrm{d}\left(\gamma_{s,i}\,\boldsymbol{v}_{s,i}\right)}{\mathrm{d}t} = \frac{q_s}{m_s}\left(\boldsymbol{E} + \boldsymbol{v}_{s,i}\times\boldsymbol{B}\right),$$
$$\frac{\mathrm{d}\boldsymbol{r}_{s,i}}{\mathrm{d}t} = \boldsymbol{v}_{s,i},$$
$$\frac{\partial \boldsymbol{E}}{\partial t} = c^2\nabla\times\boldsymbol{B} - \frac{1}{\epsilon_0}\Sigma_s\boldsymbol{j}_s,$$
$$\frac{\partial \boldsymbol{B}}{\partial t} = -\nabla\times\boldsymbol{E}.$$

Here, $\boldsymbol{v}$, $\boldsymbol{r}$, and $\gamma = \sqrt{1 - v^2/c^2}$ are the velocity, position, and Lorentz factor of the particles, and $\boldsymbol{B}$ and $\boldsymbol{E}$ are the magnetic and electric fields, respectively. c, m, q, and t are the speed of light, mass, electric charge, and time, respectively, and ϵ_0 is the permittivity of free space. The subscripts s and i denote the plasma species (s = i for ions and e for electrons) and the particle index, respectively. The particle current densities are calculated from $\boldsymbol{j}_s = \sum_i q_s \boldsymbol{v}_{s,i}$ with the shape factor of (super-) particles.

Initially, the magnetic fields are defined to satisfy the equation $\nabla\cdot\boldsymbol{B} = 0$. Then, pairs of electrons and ions are uniformly distributed throughout the simulation domain such that $\nabla\cdot\boldsymbol{E} = \rho^+/\epsilon_0$ is automatically satisfied (ρ^+ is the charge density). Therefore, the plasma is initially electrically neutral.

2.2 Initial conditions

To set the magnetic X-point in the x-y plane, the initial magnetic field is set such that

$$(B_x,\ B_y,\ B_z) = \left(\frac{B_0}{L}y,\ \frac{B_0}{L}\alpha^2 x,\ 0\right),$$

where B_0 is the magnetic field intensity at a distance L from the origin, corresponding to the X-point, for the stress parameter $\alpha = 1.0$ (L is the reconnection length scale). The stress parameter α controls the geometry of the magnetic field and the initial magnetic pressure that collapses the system in the x direction. For $\alpha = 1$, the angle between separatrixes of the magnetic field is 90°. In this paper, $\alpha = 1.2$, corresponding to the weak reconnection case used in the previous study. By taking the curl of the magnetic field, the initial uniform current density is given by

$$j_z = \frac{B_0}{\mu_0 L}\left(\alpha^2 - 1\right),$$

where μ_0 is the permeability of free space.

For $\alpha = 1$ (no stress), the current density of the system is zero, maintaining a state of equilibrium such that no reconnection occurs. By contrast, when $\alpha \geq 1$ (stressed), a current density is uniformly produced in the z direction, resulting in a force of $\boldsymbol{j}\times\boldsymbol{B}$, which begins to collapse the system in the x direction. Here, the presence of the $\boldsymbol{j}\times\boldsymbol{B}$ force disrupts the pressure balance throughout the system, which transiently exhibits a non-equilibrium state. Consequently, electric fields are produced along the direction of the uniform current flows. After a short duration, the system tends to approach equilibrium, and thus, we can evaluate the physics of magnetic reconnection in the vicinity of the X-point.

Figure 1 shows our simulation model. All other initial conditions and parameters are the same as in the previous study [5, 6]. The X-point is located at the center of our numerical domain. The solid colored lines show the magnetic field lines for $\alpha = 1.2$, which are plotted by calculating the z component of the initial vector potential.

The lengths in two dimensions are $L_x = L_y = 400\Delta$, excluding ghost cells. Δ (= 1) is the numerical grid size corresponding to an electron Debye length, $\lambda_{\mathrm{De}} = v_{\mathrm{te}}/(\sqrt{2}\omega_{\mathrm{pe}})$, where v_{te} and ω_{pe} are the electron thermal

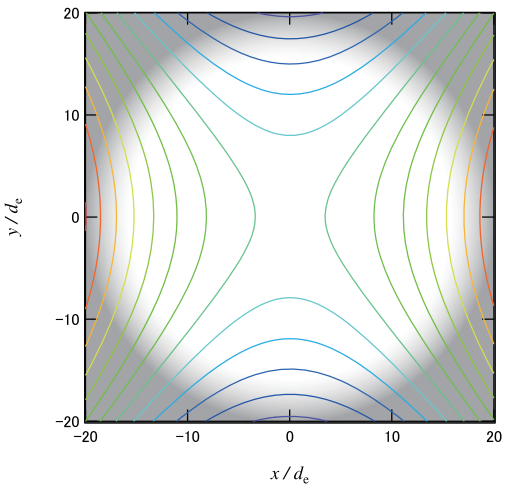

Fig. 1 Our simulation model in the x-y plane. The spatial lengths are normalized by the electron skin depth d_e. The solid colored lines show magnetic field lines for $\alpha = 1.2$. The gray-scale area shows the absorption region.

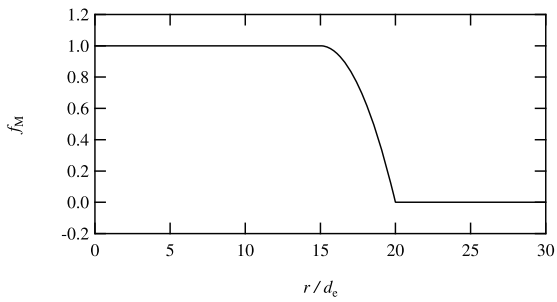

Fig. 2 The masking function f_M used to reduce the amplitudes of waves in the absorption region. The horizontal axis is the distance r (normalized by the electron skin depth) from the X-point.

speed and electron plasma frequency, respectively. The reconnection scale is $L = 200\Delta$, and the time step is taken to be $\omega_{pe}\Delta t = 0.05$, where Δt (= 1) is the time interval. The duration of our simulation is $5,000\Delta t$, corresponding to $\omega_{pe}t = 250$, and the speed of light is $c = 0.5$.

The electrons and ions are uniformly distributed throughout the numerical domain. The ion-to-electron mass ratio is chosen as $m_i/m_e = 100$, and the particle number densities are $n_e = n_i = n_0 = 100$ per grid cell. Therefore, the total particle number is 1.6×10^7 electron-ion pairs. The electron and ion skin depths are $d_e = c/\omega_{pe} = 10\Delta$ and $d_i = c/\omega_{pi} = 100\Delta$, respectively. The plasma temperatures of each species are equal, $T_i = T_e$, and thus, the electron thermal velocity is $v_{te}/c = 0.1$. Using the magnetic field intensity B_0, the ratio of the electron cyclotron frequency to the plasma frequency is set such that $\omega_{ce}/\omega_{pe} = 1.0$. The plasma beta is $\beta = 2(v_{te}/c)^2/(\omega_{ce}/\omega_{pe})^2 = 0.02$, the Alfvén velocity is $V_{A0}/c = 0.1$, and the Alfvén time is $\omega_{pi}\tau_{A0} = (L/d_i)/(V_{A0}/c) = 20$.

To produce a uniform current in the z direction, the particle drift velocity is calculated to be $v_d/c = (\alpha^2 - 1)\,(\omega_{ce}/\omega_{pe})\,(d_e/L) = 0.022$. Half of the velocity is imposed on both the electrons and ions, and therefore, their velocity distribution functions in the z direction become slightly shifted-Maxwellian.

2.3 Boundary conditions

The previous study employed the condition that neither the plasma particles (mass flow) nor the magnetic flux can pass through the boundaries [5, 6]. In this study, the boundary conditions are almost the same as those in the previous study. To fulfill this condition, zero-gradient boundary conditions are imposed on all three components of both the electric and magnetic fields in the x and y directions. In addition, the tangential component of the electric fields is forced to zero, because the normal component of the magnetic fields is held constant. Reflection boundary conditions are also imposed on all particles in the x and y directions. Moreover, in the present study, the current densities generated by the particles reflected from the boundaries are interpolated in the physical domain (just inside the boundary layers) for the sake of precise calculation. Therefore, our system is completely isolated and is thus superior to the system presented in the previous study.

The gray-scale area in Fig. 1 shows an absorption region on the outer side of the X-point. The absorption region is ordinarily used to damp (decrease) the amplitude of waves propagating outward and to suppress the reflection of waves from the boundaries. For the PIC simulation of a stressed X-point collapse, the initially induced electric fields propagate outward, are reflected from the boundaries, and then influence the reconnection physics in the vicinity of the X-point.

Figure 2 shows the masking function f_M used to damp the amplitudes of the waves in the absorption region [12]. The horizontal axis is the distance r (normalized by the electron skin depth) from the X-point, $r = \sqrt{x^2 + y^2}$. This function is described by

$$f_M = \begin{cases} 1 & (0 \le r \le L_1) \\ 1 - \left(\frac{r - L_1}{L_d}\right)^2 & (L_1 \le r \le L_2) \\ 0 & (L_2 \le r) \end{cases},$$

where L_1 (= $15d_e$), L_2 (= $20d_e$), and L_d (= $5d_e$) indicate the starting and end points and the length of the damping region, respectively. Since the masking function is applied to all three components of the electric fields present in the absorption region ($L_1 \le r$), the electric fields propagating outward vanish before they reach the edges of the simulation box.

Here, all particles are completely reflected at each edge of the simulation box ($x/d_e = 20$, $y/d_e = 20$). Although the location of particle reflection differs from the absorption region and the masking function f_M has a discontinuity at $r/d_e = 20$, as shown in Fig. 2, this method

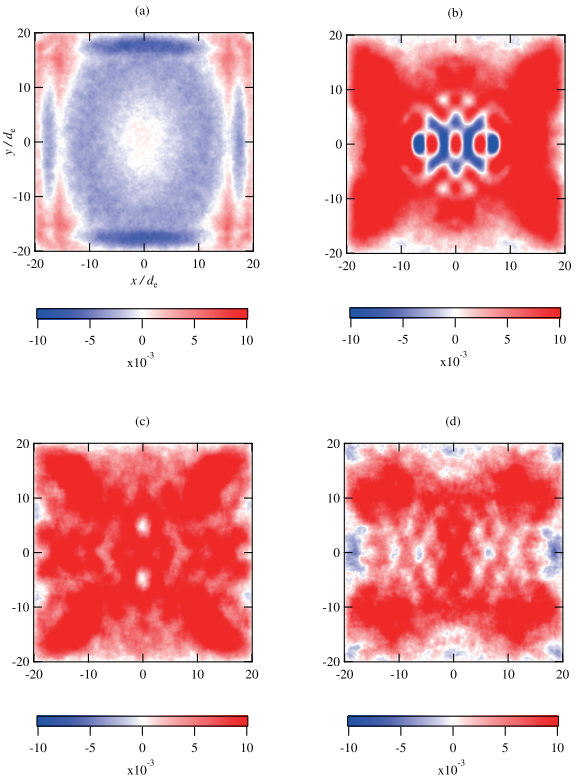

Fig. 3 Time development of the spatial distributions of the electric field E_z/E_0 at (a) $\omega_{pe}t$ = 5, (b) 50, (c) 150, and (d) 170 in the x-y plane in the absence of an absorption region.

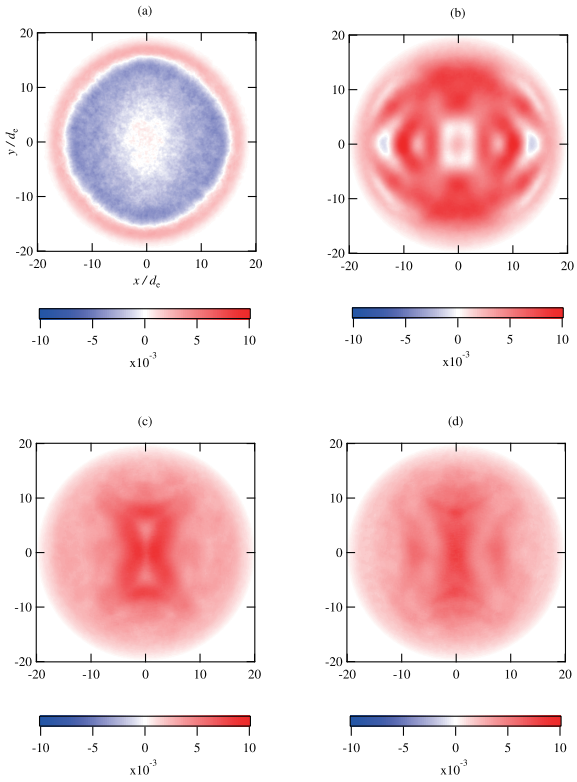

Fig. 4 Time development of the spatial distributions of the electric field E_z/E_0 at (a) $\omega_{pe}t$ = 5, (b) 50, (c) 150, and (d) 170 in the x-y plane in the presence of an absorption region.

effectively suppresses the reflection of electric fields in the present simulation.

3. Simulation Results

In this section, we discuss our simulation results and compare them to those of the previous study. We focus on whether the electric fields propagating outward are sufficiently damped by the absorption region and whether their boundary reflections are suppressed.

In this paper, the time, spatial lengths, and velocities are normalized by the inverse of the electron plasma frequency ω_{pe}^{-1}, electron skin depth d_e, and speed of light c.

Figure 3 shows the time development of the spatial distributions of the electric field E_z/E_0 at (a) $\omega_{pe}t$ = 5, (b) 50, (c) 150, and (d) 170 in the x-y plane in the absence of an absorption region. The numerical setup is the same as in the previous study. The time $\omega_{pe}t$ = 170 indicates the peak of the magnetic reconnection rate. The electric fields are normalized by $E_0 = m_e c\omega_{pe}/e$ (e is the electron charge). To emphasize these structures, the range of the color scale is fixed as −0.01 to +0.01. As shown in Fig. 3 (a), positive electric fields are observed at each corner of our simulation box. Strong negative electric fields are also observed at the edge of the y boundaries (top and bottom sides). Because these effects occur at the boundary edges/corners, we conclude that they are unphysical. In Fig. 3 (b), two arched structures are shown in both of the x boundary layers (left and right sides). A *kaleidoscope*-like structure occurs in the vicinity of the X-point, caused by the reflected electric fields, which propagate and interact with each other throughout the numerical domain. These complicated structures continue to exist, as shown in Figs. 3 (c-d).

Figure 4 shows the time development of the spatial distributions of the electric field E_z/E_0 at (a) $\omega_{pe}t$ = 5, (b) 50, (c) 150, and (d) 170 in the x-y plane in the presence of an absorption region. The absorption region is superimposed on the simulation model used in the previous study to suppress the reflection of the electric fields propagating outward. Here, we plot the entire domain, including the absorption region, to confirm the improvement of unphysical results at the boundary edges/corners and the suppression of reflected electric fields. As shown in Fig. 4 (a), a circular distribution of electric fields arises because of the effects of the absorption region. The abnormal (unphysical) electric fields at the corners and edges of the simulation box (see Fig. 3 (a)) can be absorbed, and positive electric fields begin to localize in the vicinity of the X-point in Figs. 4 (b-d). This localization is not observed in the absence of the absorption region (see Figs. 3 (c-d)).

Comparing the simulation results shown in Figs. 3 and 4, we find that abnormal results and the reflection of elec-

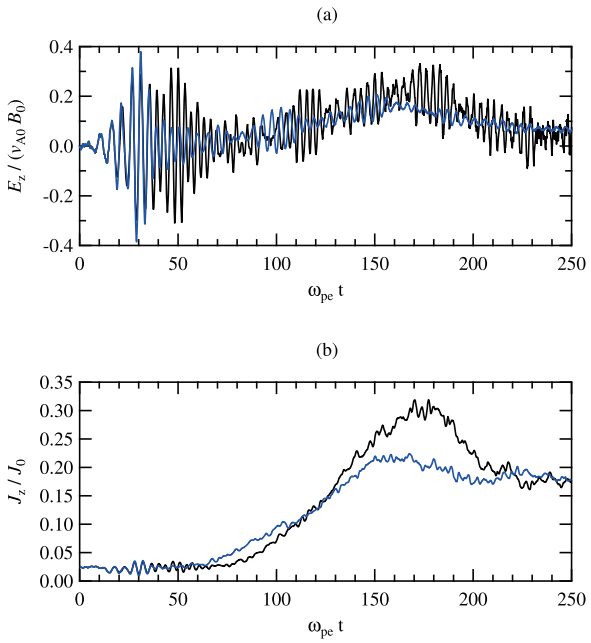

Fig. 5 Time evolution of the (a) electric field $E_z/(V_{A0}B_0)$ and (b) current density j_z/j_0 at the X-point $(x/d_e,\ y/d_e) = (0,\ 0)$. The black and blue solid lines show results obtained in the absence and presence of an absorption region, respectively.

tric fields are largely suppressed. Therefore, we conclude that the absorption region introduced in this simulation is effective for performing PIC simulations of a stressed X-point collapse.

Figure 5 shows the time evolution of the (a) electric field $E_z/(V_{A0}B_0)$ and (b) current density j_z/j_0 at the X-point $(x/d_e,\ y/d_e) = (0,\ 0)$, where the black and blue solid lines show the results obtained in the absence and presence of an absorption region, respectively. Specifically, the out-of-plane electric field at the X-point, $E_z(0,0)$, represents the magnetic reconnection rate in Fig. 5 (a). In the previous study, the reconnection rate was plotted with a boxcar average scheme to smooth the data with large fluctuations, but here, we plot the data without smoothing for comparison (see the black solid line in Fig. 5 (a)). In both the absence and presence of the absorption region, the electric fields at the X-point strongly oscillate in the early phase $(0 \le \omega_{pe}t \le 30)$ because of the electric field initially induced in the non-equilibrium state of the stressed X-point collapse. The system approaches equilibrium as the electric fields are induced. In the absence of the absorption region (previous study), the electric field gradually increases until it reaches a peak at $\omega_{pe}t = 170$. By contrast, in the presence of the absorption region (present study), the oscillation is reduced, and the peak time occurs earlier than in the previous case. We estimate that the peak shifts from $\omega_{pe}t = 170$ to 150.

Figure 5 (b) shows a portion of the current localization at the X-point. The current density is normalized by

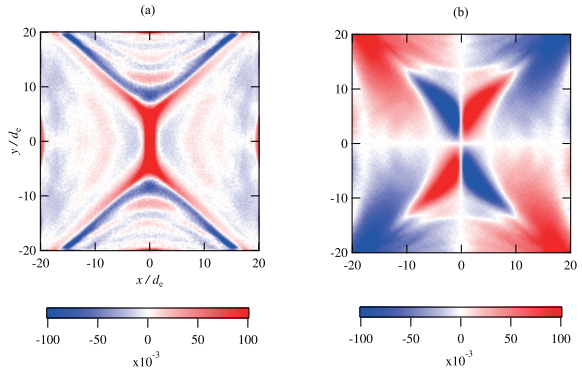

Fig. 6 Spatial distributions of (a) current density j_z/j_0 and (b) magnetic field B_z/B_0 at $\omega_{pe}t = 170$ in the absence of an absorption region.

$j_0 = n_0ec$ (note that this is different from the previous notation). It is well-known that a current sheet is produced in the vicinity of an X-point because of magnetic reconnection. In the presence of an absorption region, the current density increases slightly faster from $\omega_{pe}t = 60$, but the peak is lower compared with the result without an absorption region. We believe that the reconnection dynamics are smoother because the reflection of the electric fields was removed from the simulation.

Figure 6 shows the spatial distributions of the (a) current density j_z/j_0 and (b) magnetic field B_z/B_0 at $\omega_{pe}t = 170$ in the absence of an absorption region. Before the absorption region is imposed, electric fields propagate throughout the simulation box and are reflected from the boundaries. In Fig. 6 (a), although a current sheet is produced in the vicinity of the X-point, unphysical positive current densities are observed at the edges of the simulation box. As shown in Fig. 6 (b), a quadrupole magnetic field is observed in the vicinity of the X-point; however, thread-like structures (white regions) appear along the line $y = 0$ and near the y boundary layers. We conclude that these effects are caused by the reflection of the electric fields from the simulation boundaries.

Figure 7 shows the spatial distributions of the (a) current density j_z/j_0 and (b) magnetic field B_z/B_0 at $\omega_{pe}t = 170$ in the presence of an absorption region. Specifically, the structures of the current sheet and quadrupole magnetic field are clearer compared with Fig. 6. The abnormal electric fields observed at each edge of the simulation box and the thread-like structures outside the quadrupole magnetic field disappear. Therefore, introducing the absorption region improves the quality and clarity of our simulation of a stressed X-point collapse.

Figure 8 shows the electron energy distribution functions at $\omega_{pe}t = 170$, where the black and blue solid lines show the results obtained in the absence and presence of an absorption region, respectively. The horizontal axis $(\gamma_e - 1)$ represents the relativistic electron kinetic energy normalized by the rest mass energy. The vertical axis f_e is the

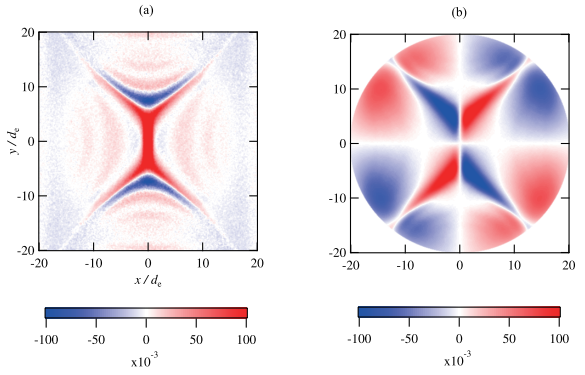

Fig. 7 Spatial distributions of (a) current density j_z/j_0 and (b) magnetic field B_z/B_0 at $\omega_{pe}t = 170$ in the presence of an absorption region.

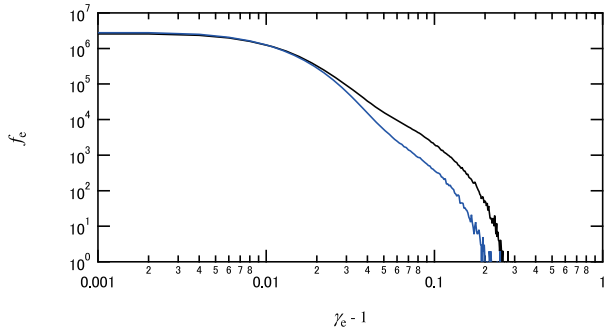

Fig. 8 Electron energy distribution functions at $\omega_{pe}t = 170$. The black and blue solid lines show results obtained in the absence and presence of an absorption region, respectively.

electron energy distribution function, corresponding to the number of electrons. The black solid line in Fig. 8 shows that electrons are abnormally accelerated and/or heated in the absence of an absorption region compared with the blue solid line. This result occurs because the electric fields reflected from the boundaries can accelerate the electrons throughout the domain. However, the blue solid line in Fig. 8 shows the accurate non-thermal electron acceleration since the introduced absorption region can suppress the reflection of electric fields.

4. Conclusions

To suppress the reflection of the electric fields propagating outward, an absorption region was superimposed on the simulation model used in a previous study. In particular, a masking method is employed in the absorption region to strongly damp the amplitude of the electric fields propagating outward and then to suppress their reflection from the boundaries. As a result, the influence of the reflected electric fields on the X-point is removed from the system. The strong oscillation of the reconnection rate is weakened, and the reconnection physics become moderate in comparison with those of the previous study. The structures of the reconnection current sheet and quadrupole magnetic fields are clarified. Hence, the introduction of an absorption region is highly effective for investigating the underlying physics of a stressed X-point collapse.

Hereafter, we will be able to analyze the behavior of energetic plasma particles in precise PIC simulations of a stressed X-point collapse. Note that the introduction of an absorption region, with a damping length of $L_d = 50\Delta$, reduces the physical domain size. Therefore, we must increase the simulation size to account for the absorption region. Moreover, when considering the z direction, the trajectories of particles (particularly electrons) will be cleared along with a reconnection electric field. Competition between the traditional outflow (in the y direction) and direct acceleration by the reconnection electric field (in the z direction) is a subject of future research.

[1] E. Priest, T. Forbes, *Magnetic Reconnection: MHD Theory and Applications* (Cambridge University Press, Cambridge, 2000).
[2] D. Biskamp, *Magnetic reconnection in plasmas* (Cambridge University Press, Cambridge, 2000).
[3] J. Birn, J.F. Drake, M.A. Shay, B.N. Rogers, R.E. Denton, M. Hesse, M. Kuznetsova, Z.W. Ma, A. Bhattacharjee, A. Otto and P.L. Pritchett, J. Geophys. Res. **106**, 3715 (2001).
[4] P.L. Pritchett, J. Geophys. Res. **106**, 3783 (2001).
[5] D. Tsiklauri and T. Haruki, Phys. Plasmas **14**, 112905 (2007).
[6] D. Tsiklauri and T. Haruki, Phys. Plasmas **15**, 102902 (2008).
[7] J. Graf von der Pahlen and D. Tsiklauri, Phys. Plasmas **21**, 012901 (2014).
[8] J. Graf von der Pahlen and D. Tsiklauri, Astron. Astrophys. **595**, A84 (2016).
[9] J.G. von der Pahlen and D. Tsiklauri, Phys. Plasmas **21**, 060705 (2014).
[10] J. Graf von der Pahlen and D. Tsiklauri, Phys. Plasmas **22**, 032905 (2015).
[11] S. Zenitani and T. Nagai, Phys. Plasmas **23**, 102102 (2016).
[12] T. Tajima and Y.C. Lee, J. Comput. Phys. **42**, 406 (1981).
[13] O. Buneman, *Computer Space Plasma Physics: Simulation Techniques and Software*, edited by H. Matsumoto and Y. Omura (Terra Scientific, Tokyo, 1993) p. 67.